Journal of the Mechanics and Physics of Solids 60 (2012) 1350–1362

Contents lists available at SciVerse ScienceDirect

Journal of the Mechanics and Physics of Solids

journal homepage: www.elsevier.com/locate/jmps

Transient creep effects and the lubricating power of water in materials ranging from paper to concrete and Kevlar

Ivan Vlahinić [a,*], Jeffrey J. Thomas [b], Hamlin M. Jennings [c,**], José E. Andrade [d]

[a] Northwestern University, Evanston, IL 60208, USA
[b] Schlumberger-Doll Research, Cambridge, MA 02139, USA
[c] Massachusetts Institute of Technology, Cambridge, MA 02139, USA
[d] California Institute of Technology, Pasadena, CA 91125, USA

ARTICLE INFO

Article history:
Received 31 May 2011
Received in revised form
24 February 2012
Accepted 3 March 2012
Available online 16 March 2012

Keywords:
Viscosity
Creep
Cyclic changing moisture
Pore fluid
Double dual porosity diffusion

ABSTRACT

A diverse class of viscous materials, which includes familiar materials such concrete, wood, and Kevlar, exhibit surprising, counterintutive properties under internal moisture content fluctuations. In test after test over the past 50 years, the viscosity of these materials is observed to decrease, often dramatically, during wetting and drying. The key characteristics of the observed viscous softening are: the decrease in viscosity is temporary, and depending on the specimen size can be greatly delayed with respect to the associated change in weight; the decrease in viscosity is absent under steady state flow.

Based on recent research on the properties of water and other polar fluids confined by hydrophilic surfaces, we provide a physical explanation and propose a constitutive law. The resulting model accurately captures the interplay between the pore fluid movement and macroscopic constitutive properties in totality. The model is verified against published data for the creep of paper sheets exposed to cyclic moisture conditions. Experimental data of different materials under similar boundary conditions are compared using a new metric, the creep rate factor. The results further reinforce the idea that nanoscale movement of water enhances the internal 'lubrication' of the studied materials, interpreted as loosening of the hydrogen bonds.

1. Introduction

1.1. General background

The viscosity is a measure of internal resistance to 'flow', a material property attributable to both liquids and solids alike. In porous hydrophilic materials, the viscosity characterizes the composite property of the solid and pore phases. Its value is generally dependant on the moisture content, a mass ratio between pore water and the solid phase, such that the creep rate (the rate of strain under constant load) is generally greater at higher moisture content. This behavior can be attributed to the ability of water to lubricate internal interfaces within these materials. However, *transient* moisture conditions, i.e. changes in the internal moisture content (MC) or relative humidity (RH) level with time, produce unexpected and often counterintuitive behavior. For example, a specimen dried while under load would be expected to exhibit a steadily declining creep rate due to a progressive loss of internal lubrication. In fact, for many materials the creep rate temporarily increases during drying, often reaching values that

* Corresponding author. Present address: California Institute of Technology, Pasadena, CA 91125, USA. Tel.: +1 626 395 8157.
** Corresponding author. Tel.: +1 617 253 7127.
E-mail addresses: ivan@caltech.edu (I. Vlahinić), JThomas39@slb.com (J.J. Thomas), hmj@mit.edu (H.M. Jennings), jandrade@caltech.edu (J.E. Andrade).

0022-5096/$ - see front matter © 2012 Elsevier Ltd. All rights reserved.
http://dx.doi.org/10.1016/j.jmps.2012.03.003

are several times the initial creep rate, before declining to the expected steady-state level as the internal moisture state equilibrates. Similar trends are evident during wetting. In one extreme case, exposure of a dry wool fiber to moist (94% relative humidity) air induced a temporary state of nearly complete torsional plasticity (Mackay and Downes, 1959). In other words, the fiber temporarily lost all ability to resist load.

Transient mechanical responses to changes in MC have been observed during static, cyclic, and dynamic tests, and under essentially all loading conditions, including axial tension and compression, torsion, bending, and shear. That is not to say that every material has been tested under all loading scenarios. Specimen shape and size place practical limits on the type of loading that can be applied, e.g. thin cylindrical fibers have a natural predisposition for tensile and torsional tests. Nevertheless, the tests collectively indicate that the said phenomenon is clearly independent of the loading type.

Historically, the first published observation of the transient phenomenon appears to be that of Pickett (1942) nearly 60 years ago, who noted that the deformation of concrete during simultaneous drying and loading exceeded the sum of the individual effects. This well-known 'Pickett effect' has never been fully explained despite extensive study of the physical and mechanical properties of concrete. Since that study, transient moisture-induced mechanical effects have been reported for a wide range of materials (outlined below) and described using a variety of terminology including *drying creep*, *stress-induced shrinkage*, *mechano-sorptive creep*, and *moisture induced* or *accelerated creep*. Organic and inorganic materials exhibiting this general type of effect include:

calcium–silicate–hydrate (*C–S–H*): cement paste (Bažant et al., 1976), concrete (Pickett, 1942; Vandamme and Ulm, 2009), and other cement-based materials;
cellulose: wood (Armstrong and Kingston, 1960; Armstrong and Christensen, 1961), wood fibers (Olsson et al., 2007), corrugated fiberboard (Söremark and Fellers, 1993; Urbanik, 1995), plywood (Haygreen et al., 1975), paper (Byrd, 1972; Alfthan, 2004), ramie fibers (Chinese grass), lyocell fiber (regenerated cellulose), and cellophane (Habeger et al., 2001);
keratin: sheep wool fibers (Mackay and Downes, 1959; Feughelman, 1962; Nordon, 1962) and horse hair (Danilatos and Postle, 1981);
synthetic or semi-synthetic polymers: polyurethane foam (Dounis et al., 1993), Kevlar® (Wang et al., 1990; Habeger et al., 2001), Technora® and Twaron® (Wang et al., 1992), and nylon-66 (Liou, 1998; Habeger et al., 2001) fibers, their composites, and others (Kubát and Lindbergson, 1965).

1.2. A common metric: creep rate factor

Experimental findings of this diverse group of materials, ranging from amorphous (or at best poorly crystalline) in the case of C–S–H to strongly crystalline in the case of Kevlar, show qualitatively similar behavior. For a direct quantitative comparison, we must first introduce a common non-dimensional metric. To this end, we additively decompose the total strain rate $\dot{\varepsilon}$, into the elastic $\dot{\varepsilon}^e$ and viscous components:

$$\dot{\varepsilon} = \dot{\varepsilon}^e + c\dot{\varepsilon}^v \quad \text{where } c = 1 + \frac{\dot{\varepsilon}^\star}{\dot{\varepsilon}^v} \tag{1}$$

where $\dot{\varepsilon}^v$ is the viscous strain rate under steady-state moisture and $\dot{\varepsilon}^\star$ is the additional transient viscous strain rate. As a sole modification to the classic form, we define the dimensionless creep rate factor c. Note that c takes on a value of unity whenever the internal moisture equilibrium is attained. In this way, the creep rate factor isolates the material response to *changes* in moisture content, i.e. the transient effects. The calculated values of c from experiments of cement paste, wood, and Kevlar/epoxy composite are shown in Fig. 1, indicating striking quantitative similarities.[1]

In addition to the referenced materials, there are other intriguing candidate materials as well. The viscous response of silkworm silk (Pérez-Rigueiro et al., 2000), spider dragline silk (Smith et al., 2003; Ritchie et al., 2005), rabbit ligament (Chimich et al., 1992; Thornton et al., 2001), human tendon (Haut and Haut, 1997; Atkinson et al., 1999), regenerated collagen film (Tanioka et al., 1973), and bone (bovine, Sasaki and Enyo, 1995, and human, Garner et al., 2000) are all strongly influenced by their steady state MC but apparently have not yet been tested under transient conditions.

1.3. Perspective on the physical origins of viscous softening

Several explanations of the transient phenomenon have been advanced over the years, some quantitative. Many are described in a review by Wang et al. (1991), which, although generally excellent, overlooks an extensive body of literature of cementitious materials. And while there is a general agreement that the origin of the steady-state viscous response is a slip at the smallest material scales, little agreement exists on the origin of transient phenomenon, even within literature of any one material. The proposed explanations for the most part can be divided into two main camps: (1) Drying/wetting produces internal differential stresses, either due to a finite cross-sectional thickness and/or due to a presence of solid phases with different material properties. The end result of differential stresses is excess deformation under constant load,

[1] It would be even better to express time in Fig. 1 as a dimensionless or characteristic time (e.g. see Eq. (A.4a)). This would require knowledge of the (macro) diffusivity of the cited materials, a quantity not reported in and not easily inferred from the referenced works.

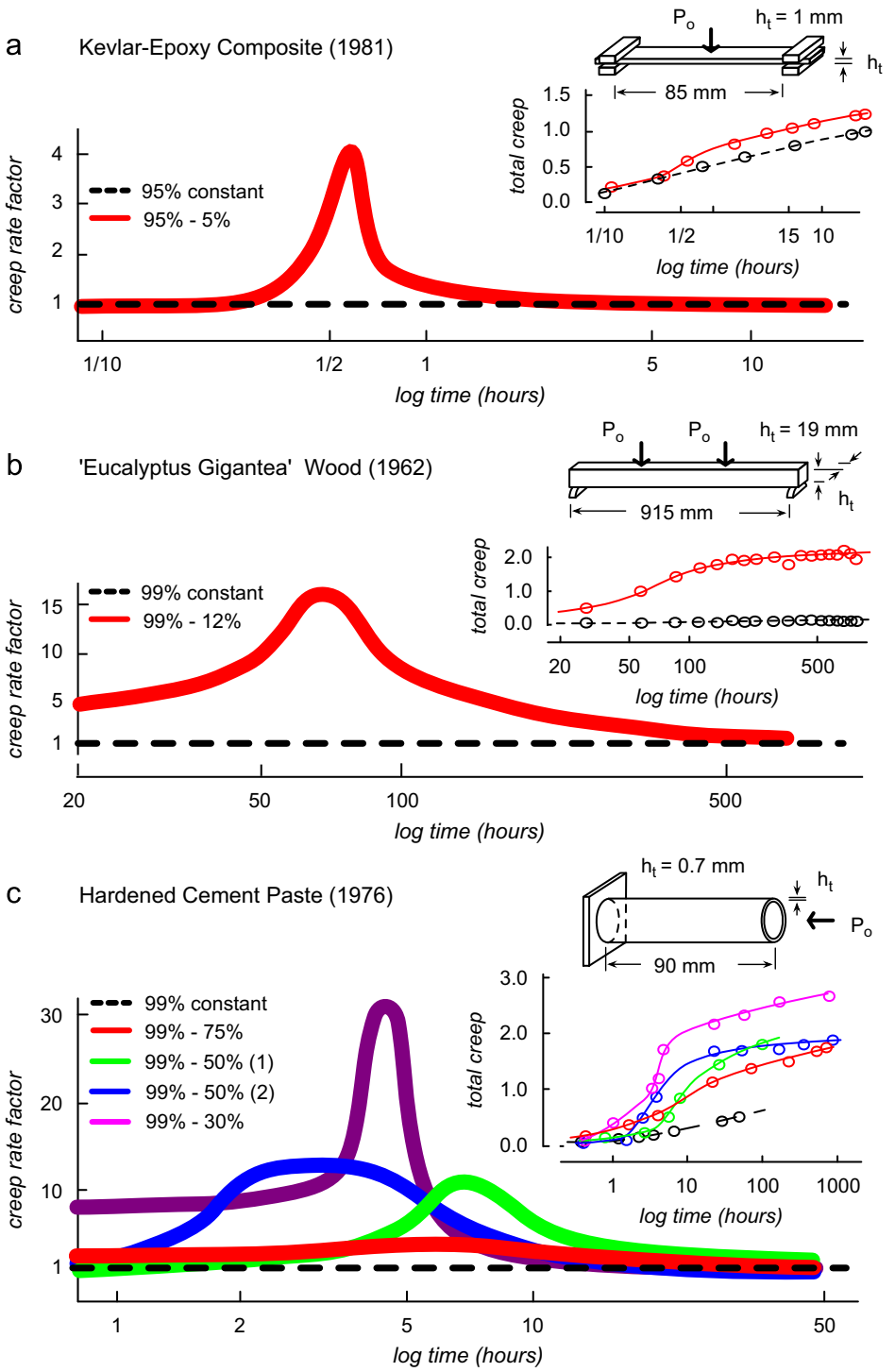

Fig. 1. Effect of ambient relative humidity change on the macroscopic creep behavior of (a) Kevlar/epoxy composite (Wang et al., 1990), (b) wood (Armstrong and Kingston, 1962), and (c) hardened cement paste (Bažant et al., 1976). The values of creep rate factor c greater than 1 indicate that the viscosity of the material is decreasing or equivalently, that the rate of creep is increasing due to internal moisture movement (see definition in Eq. (1)). The relative symmetry of the creep rate factor in log time plot is indicative of a diffusion related phenomenon. All tests were performed under static load on initially saturated specimens (sketch of experimental setup shown alongside). Inset: the open circles are the experimental data points and the solid lines are guides to the eye. For tests conducted under bending (wood and Kevlar-epoxy), the total creep is given as a fraction of the initial elastic deflection at center span, rather than of the initial elastic strain (cement paste) for test under uniaxial compression. Main: the solid lines are based on our calculations of the creep rate from the changes in total creep with time. Note that the time of maximum creep rate occurs well after the start of drying (time zero) and in general need not coincide with the time of maximum rate of moisture loss (see Section 4.1). These key features are captured by the model presented in this paper.

provided that the material-point creep response is non-linear, as first proposed by Pickett (1942) or provided that the stresses cause permanent material damage, e.g. cracking (Bažant and Xi, 1994). (2) Drying/wetting initiates the internal movement of water, which disturbs a natural equilibrium of existing molecular bonds. The end result is that under constant load, the 'disturbed' bonds will tend to more easily slip into a new favorable configuration, resulting in excess deformation, as first proposed by Gibson (1965). As of yet, neither hypothesis has been able to fully explain the key characteristics of the transient creep observed in different materials.

The aim of this paper is to understand the physical mechanism controlling the transient creep response and, on this basis, to develop a continuum model that can quantitatively reproduce its key characteristics. The contribution is rooted in the recent studies on confined fluid films and observed similarities among what are very different materials exhibiting the effect.

2. Transient creep mechanism: shear-thinning of nano-confined water

2.1. Diffusion into weak secondary bonds

We first note that all materials exhibiting the transient creep effects are porous, such that fluids can move in and out of the material and access all of the microstructure. All are composed of nanoscale 'structural units' in some sense, with mechanical properties that depend on relatively weak secondary bonds that connect them. Critically, smaller amounts of polar molecules, typically H_2O, can diffuse into and out of the nanometer-scale spaces between the 'structural units', but this process is much slower than the rate of transport through the bulk. The key is that there is a significant increase in the lubricating effect of water as it moves in and out of these nanoscale regions of the material, i.e. when the internal MC of the specimen is changing, which allows for an easier rearrangement or slip in response to a load. This mechanism is supported by recent theoretical and experimental studies of the nanoscale properties of confined fluid films, discussed in Section 2.2.

Note that the word 'structural unit' has not been formally defined. Here we mean a basic structural component of the material at the scale of a few nanometers. Physically, it may be interpreted as individual C–S–H nanoparticles in cement-based materials, microfibrils in cellulose-based materials, or individual polymer chains in the case of polymeric materials.

2.2. Fluids in a nanoscale environment

Fluids confined in nanoscale environments become structured, which strongly affects their properties. Manias et al. (1996) found that when oligomer lubricants are statically confined to dimensions comparable to their molecular size, their apparent viscosity increases dramatically. However, at even moderate shear rates, the apparent viscosity of confined lubricants decreases, approaching the bulk value at sufficiently high shear rates. Importantly, the overall response was found to depend very little on the molecular architecture, but was greatly affected by the degree of surface attraction (Manias et al., 1996). This dependence of viscosity on shear rate, termed shear-thinning, is reminiscent of pseudoplastic fluids such as paint and blood on the macroscopic scale, and has been observed in dry granular systems on the mesoscale (e.g. 50 μm glass beads, Jop et al., 2006).

Similar behavior has also been inferred from experimental and theoretical studies of water confined between attractive (hydrophilic) surfaces. Under static or quasi-static confinement, the viscosity of water is generally observed to increase once the opposing surfaces approach to within 3–7 molecular diameters (0.9–2.0 nm). The viscosity then increases by several orders of magnitude as the surfaces approach further (Li et al., 2007; Riedo, 2007), apparently as a result of increased hydrogen bonding (Major et al., 2006). The structure of resulting molecular water film has been described as ice-like, as it can be distinguished from bulk water by a sharp drop in diffusion constant, a sharp increase in shear viscosity, and by its finite shear strength (Sendner et al., 2009). The key is that the molecular dynamics simulations (Leng and Cummings, 2005) also indicate that the confined water layers exhibit shear thinning with a viscosity approaching the bulk (Newtonian) value at high shear rates.

Together, the cited studies confirm the effectiveness of water as a molecular lubricant, with properties that rival engineered oil-based lubricants (Urbakh et al., 2004), and provide an explicit physical mechanism to explain both the static and dynamic effects of moisture on the viscosity of hydrophilic nanoporous materials. Armed with this understanding, we next describe the fluid transport in a drying/wetting nanoporous medium and incorporate findings into a constitutive model, before providing the experimental validation.

3. Fluid transport in a nanoporous medium

3.1. Two scales of diffusion: physical description

The simplest description of a porous material is a two-phase medium composed of an *impermeable* solid phase and pore spaces. However, for materials exhibiting transient creep effects, the solid phase itself is also permeable. A correct material description thus requires accounting for the contrast in hydraulic properties of the two pore systems. In other words, water or other fluids should be able to macrodiffuse relatively easily but access the nanosites, i.e. the sites of secondary bonding within the solid phase, only at a much slower rate, due to the nature and close proximity (and possibly tortuosity) of the internal solid surfaces.

We note that in the remainder of this paper, a distinction between the slower-diffusing and faster-diffusing pore systems is made using the terms 'nanosites' and 'macropores' respectively. While use of these terms provides for the simplicity of discussion and ease of illustration, the language may not be directly translated to all cited materials.

In cement-based and wood-based materials, the term 'macropore' may be found throughout the literature. But what is a macropore in the context of polymers for instance? Or more precisely, what distinguishes the nanosites from the macropores in these materials? The answer to this is not straightforward and we offer one possible interpretation.

Few polymers are entirely crystalline. Polymers generally consist of amorphous and crystalline fractions, where the grain boundaries are formed by inhomogeneities in the packing of crystallites. This description suggests that macrodiffusion could take place along the relatively open grain boundaries, while the nano-diffusion could be associated with water (or other pore fluids) penetrating via the surface layers of the crystallites. Ample experimental evidence suggests that it is indeed the case for Kevlar (Mooney and MacElroy, 2007), a polymer that is perhaps the most crystalline and the least porous of the materials cited here. More generally, the preceding discussion indicates that a completely satisfactory distinction between macropores and nanosites is likely to be material specific.

3.2. Two scales of diffusion: mathematical model

A related material description for which a mathematical treatment has already been well developed and validated, albeit on a much larger scale, is the flow of fluids through fractured aquifers and petroleum reservoirs (Barenblatt and Zheltov, 1960; Chen, 1989), where the relatively open fractures permit much more rapid transport than the surrounding porous matrix. Transport in such a system can be described via coupled (fluid) mass conservation:

$$\frac{\partial w_1}{\partial t} + \mathrm{div}(\rho V_1) - q^* = 0 \tag{2a}$$

$$\frac{\partial w_2}{\partial t} + \mathrm{div}(\rho V_2) + q^* = 0 \tag{2b}$$

where subscripts 1 and 2 represent 'fast' and 'slow' flow conduits, w is the moisture concentration, V is the fluid seepage velocity, ρ is the fluid density, and q^* is the rate of fluid exchange between the two pore regions, which is proportional to their pressure difference:

$$q^* = \frac{\alpha}{\mu}(p_2 - p_1) \quad \text{where } \alpha = \frac{\kappa_2}{l^2} \tag{3}$$

where μ is the fluid viscosity, p is the pressure, κ_2 is the permeability, and l is the intrinsic or characteristic length scale of the porous matrix. The dimensionless constant α describes how easily fluid can exchange between the two pore regions. Eqs. (2) and (3) are analogous to the classic laws of heat (Fourier) transport or electrical charge (Ohm) transport when the host medium is a two phase material with each phase characterized by a thermal or electrical (as opposed to hydraulic) conductivity.

It is important to emphasize that the water in a nanosites system remains liquid at all but extremely low partial pressures as it is well ordered and tightly bound to the surfaces (Riedo, 2007; Lane et al., 2008). On the other hand, a macropore system is partially saturated with the transport driven by the gradient in the vapor pressure of pore water. The assumption that water transport in the nanosites is governed by Darcy's law and in the macropores by Fick's law leads to a set of coupled differential equations based on Eqs. (2) and (3) that describe the macropore relative humidity h_1 (rather than pressure) and the nanosite pressure p_2, as a function of both time and position within the specimen. The relation between the liquid pressure and pore humidity is furnished by the Kelvin–Laplace equation. Converting h_1 and p_2 to dimensionless variables f and g normalized with respect to boundary conditions allows them to be compared directly. A complete derivation of the described transport model, and precise definitions of f and g, are given in Appendix A.

An important physical characteristic that is captured by the transport model is the different rates at which moisture equilibrium is established within the two pore systems following a change in ambient relative humidity. Specifically, equilibration of the nanosites generally lags behind that of the macropores, as access to the nanosites is impeded, and this observation holds whether the external relative humidity is increasing or decreasing. A sample breakthrough curve illustrating this time lag is shown in Fig. 2c.

Different rates of equilibrium also lead to an overall size effect. This arises because, on the one hand, the rate at which the equilibrium is established between the macro- and the nano-pore systems is fixed for a given material. Meanwhile, the rate at which the equilibrium is established between the ambient and the macropores depends on the specimen size, which is variable. The former holds a key to the viscous softening observed at the macroscale as noted in Section 2.2 and further discussed in Section 4.1. To be clear, the size effect here refers to the *relative time delay* between the transient creep rate (equiv. a measured increase in macroscopic creep rate) and the rate of weighloss/gain (equiv. macroscopic rate of waterloss/gain). We revisit this topic in the next section, following the presentation of the constitutive model, and indeed show that the described size effect correlates remarkably well with experimental data.

4. Proposed constitutive law and validation

4.1. Constitutive law for transient viscous softening

As previously discussed, a molecular film of water trapped between the opposing solid surfaces exhibits strong shear thinning, i.e. it provides a powerful lubricating effect when the adjacent solid surfaces undergo shearing motions. Here we

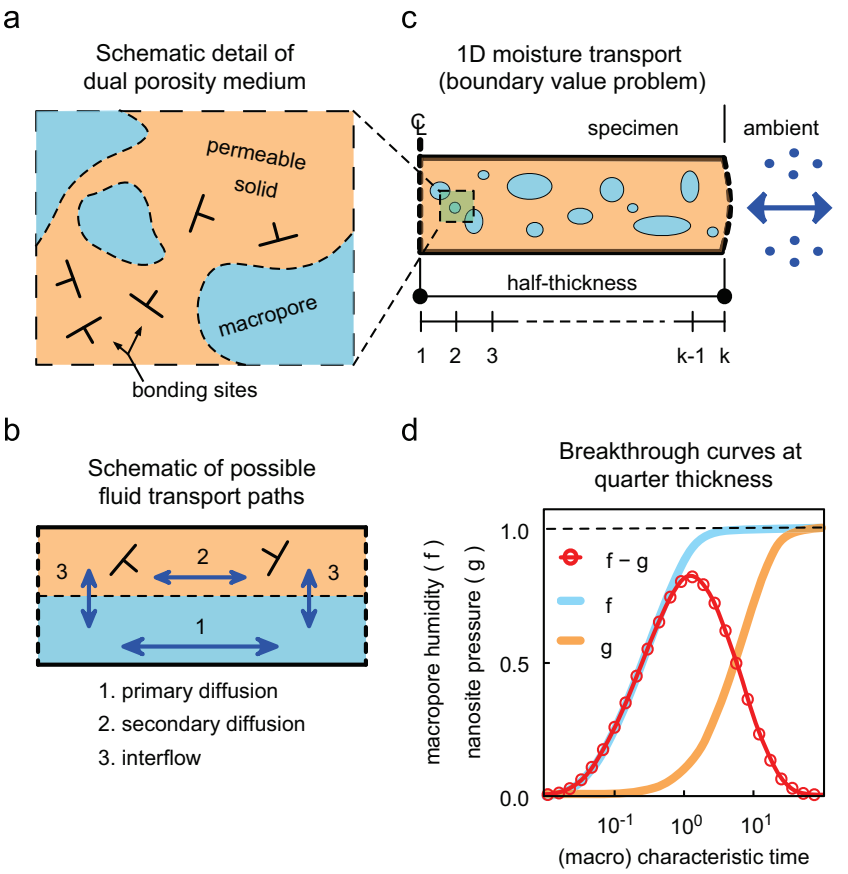

Fig. 2. Modeling fluid transport in a dual porosity medium. (a) Schematic of a microstructure with permeable solid phase. Macropores provide relatively fast flow conduits for pore water, while access to the secondary bonding sites within the solid phase is possible only at a much slower rate. (b) Possible pore water transport paths through the material in (a). Where significant contrast exists between the primary and secondary diffusive paths, access to the secondary bonding sites is controlled by the rate of fluid interflow (3). (c) 1D boundary value problem discretized into k nodes. A finite difference routine can be used to solve for the macropore relative humidity and the nanosite fluid pressure at each node as a function of time (refer to Appendix A for numerical treatment). (d) Sample breakthrough curve at the quarter-thickness. Difference between the normalized macropore humidity (f) and normalized nanopore pressure (g), reflects the time lag that arises from the different rates at which equilibrium is established within the two pore systems following a change in external relative humidity. Note that characteristic time is dimensionless, as defined in Eq. (A.4a).

note that movement of the water itself relative to the surfaces will have an equivalent, if not an enhanced effect. Thus, we argue that the most pertinent variable affecting the macroscopic mechanical response of the material is the rate of fluid movement into or out of the bonding sites within the solid phase. In terms of the transport model introduced in the previous section, this is the fluid interflow, $q^\star$. We therefore propose the following constitutive law:

$$\frac{\eta^\star}{\eta^v} = \frac{1}{k|q^\star|} \tag{4}$$

where $\eta^\star$ is the transient material viscosity, η^v is the material viscosity under steady-state moisture conditions, and k is a constant. Defining Eq. (4) in terms of the absolute value of $q^\star$ ensures that the viscous softening is independent of the flow direction. Together with the transport model based on Eqs. (2) and (3), this simple constitutive description explains the key transient creep characteristics observed at the structural level of the material. A method of loading also plays a role in determining the overall structural response. However, examining experimental data on the extremes of very thin and very thick specimen, important physical characteristics of transient phenomenon can be deduced that are independent of the loading mode:

Absence of viscous softening under steady-state moisture transport: Experiments on hollow-core wood samples under compression have long found that a specimen under a steady state moisture gradient (induced by a constant difference between the interior- and exterior-core relative humidity) exhibits no viscous softening (Armstrong, 1972). According to our model, at steady state, equilibrium exists between the nano- and the macro-pore systems at every material point. As a result, $q^\star$ is null throughout and the value of transient viscosity $\eta^\star$ approaches infinity (equiv. the rate of transient creep is null), in agreement with experimental data.

Instantaneous viscous softening in thick specimen: Thick specimen equilibrate slowly. More precisely, macropores in thick specimen collectively reach the ambient state slowly enough so that the internal equilibrium between the macro- and nano-pore systems at each material point has enough time to catch up. On a material point scale, for concrete members measuring centimeters or more in diameter, a law linearly coupling the strain rate and the rate of change of (macro)pore humidity was shown to capture well a range of historical data (Bažant and Chern, 1985). On the structural scale, bending tests on wood (thickness ≈ 2 cm) have shown that viscous deformations respond instantly to measured changes in specimen weight (Armstrong and Kingston, 1962, Fig. 3) (recall that weight change is a proxy for loss/gain of pore water). According to our model, if one were to observe the interflow $q^\star$ at a material point in a cross-section, $q^\star$ would first rise from and then fall back to zero 'infinitely fast' during an increment of macropore humidity. In other words, the equilibrium between the nano- and macro-pore systems would take place much faster than the equilibrium between the ambient and the macropores. And since this takes place at every material point, the overall conclusion is that in thick specimen the transient creep rises in tandem with the specimen weightloss, in agreement with experimental data.

Delayed viscous softening in thin specimen: Thin specimen equilibrate quickly. More precisely, macropores in thin specimen reach the ambient state quickly enough that the internal equilibrium between the macro- and nano-pore systems has not had time to catch up. The electrical conductivity experiments on keratin fibers support this viewpoint (Algie et al., 1960; Algie and Watt, 1965), and have shown that water is mobile internally even after macropores reach an equilibrium with the ambient (equiv. the point at which the specimen weight has more or less stabilized). Experiments also indicate that the internal pore water mobility also appears responsible for transient creep. Damping measurements (tensile and torsional) on thin fibers of paper (Kubát and Lindbergson, 1965) and keratin (Mackay and Downes, 1959; Danilatos and Postle, 1981), ranging in thickness from about 50 to 200 μm, have shown that the mobility of the molecular structure of these materials (equiv. the material's propensity to creep) also remains higher than the equilibrium value long after the macropores have equilibrated. According to our model, if one were to observe the interflow $q^\star$ at a material point in the cross-section, $q^\star$ would no longer rise from and then fall to zero 'infinitely fast' during an increment of macropore humidity. This is because in thin specimen, the time to equilibrium between the macro- and the nano-pore systems is comparable to time to equilibrium between the macropores and the ambient. The overall observation is that in thin specimen the transient creep *does not* rise in tandem with and may be significantly delayed with respect to specimen weightloss, leading to the size effect, in agreement with experimental data.

We note that our constitutive picture in Eq. (4) is approximate, but only in its detail. This is because we are using a very simple linear description of shear-thinning—the molecular dynamics experiments on various molecular lubricants indicate a logarithmic dependence of viscosity on shear rate (see e.g. Fig. 2 in Leng and Cummings, 2005 and Fig. 2 in Manias et al., 1996). The overall structure of our model is still correct and the same basic conclusions are obtained with the more complex constitutive descriptions, the use of which cannot be justified at this time.

4.2. Validation of the proposed model: uniaxial tension of paper sheet

We validate our model using the published data of Alfthan (2004) for creep of 30 μm thick paper sheets subjected to cyclic moisture conditions (see Fig. 3). Each specimen was exposed to several humidity cycles, with the start of each cycle corresponding to a very different value of the steady-state viscosity, or creep-rate, which provides a robust challenge for the model. The ambient humidity was cycled gradually, with each humidity step taking 25 min to complete while the characteristic drying/wetting time was estimated at less than 2 min. This meant that MC of the macropores follows the ambient humidity closely (see Fig. 3a), which limits the stress inhomogeneities during drying and wetting. We note that experiments of this type, i.e. well designed creep tests of thin specimen utilizing pauses between gradual humidity cycles, are extremely rare if not unique in the literature. Such experiments are also nearly impossible in some materials, e.g. in concrete where the aggregate size controls the minimum specimen size or even in cement paste where due to its quasi-brittle nature the smallest specimen tested to date appear to be those shown in Fig. 1c.

Fig. 3b shows a model fit to strain data for paper cycled between 80% and 40% RH. Only two model parameters were varied: the constitutive constant k from Eq. (4) and the hygral expansion coefficient β, which relates the rate of MC change to the rate of elastic strain and which was not reported in the original work (Alfthan, 2004). Only one parameter, the constitutive constant k, isolates the transient creep and accounts for the difference between the strains during constant and cyclic moisture conditions. All other parameters were either provided in Alfthan (2004) or estimated from other sources (see Appendix B). Using the same values for all material parameters, we then predict the total strains developed during 80–60% and 80–70% RH moisture cycling in Fig. 3d, showing that our model is sensitive to changing boundary conditions.

The total uniaxial strain of paper is determined by integrating in time the total strain rate as

$$\dot{\varepsilon} = \dot{\varepsilon}^e + c\dot{\varepsilon}^v = (\beta)\Delta h + (1 + k|q^\star|)\dot{\varepsilon}^v \tag{5}$$

where $\dot{\varepsilon}^v$ is the viscous strain rate under steady-state moisture condition and Δh is the change in relative humidity with respect to an initial reference. Viscous part of Eq. (5) is found by inserting Eq. (4) into Eq. (1), with $\dot{\varepsilon}^v$ nearly constant in log time as shown by the (diamond) data points in Fig. 3b.

The creep rate factor c is the sole modification to the classic form of Eq. (5), with values greater than 1 indicating the viscous softening of the material due to transient moisture movement. The calculated values of c from the model fit in

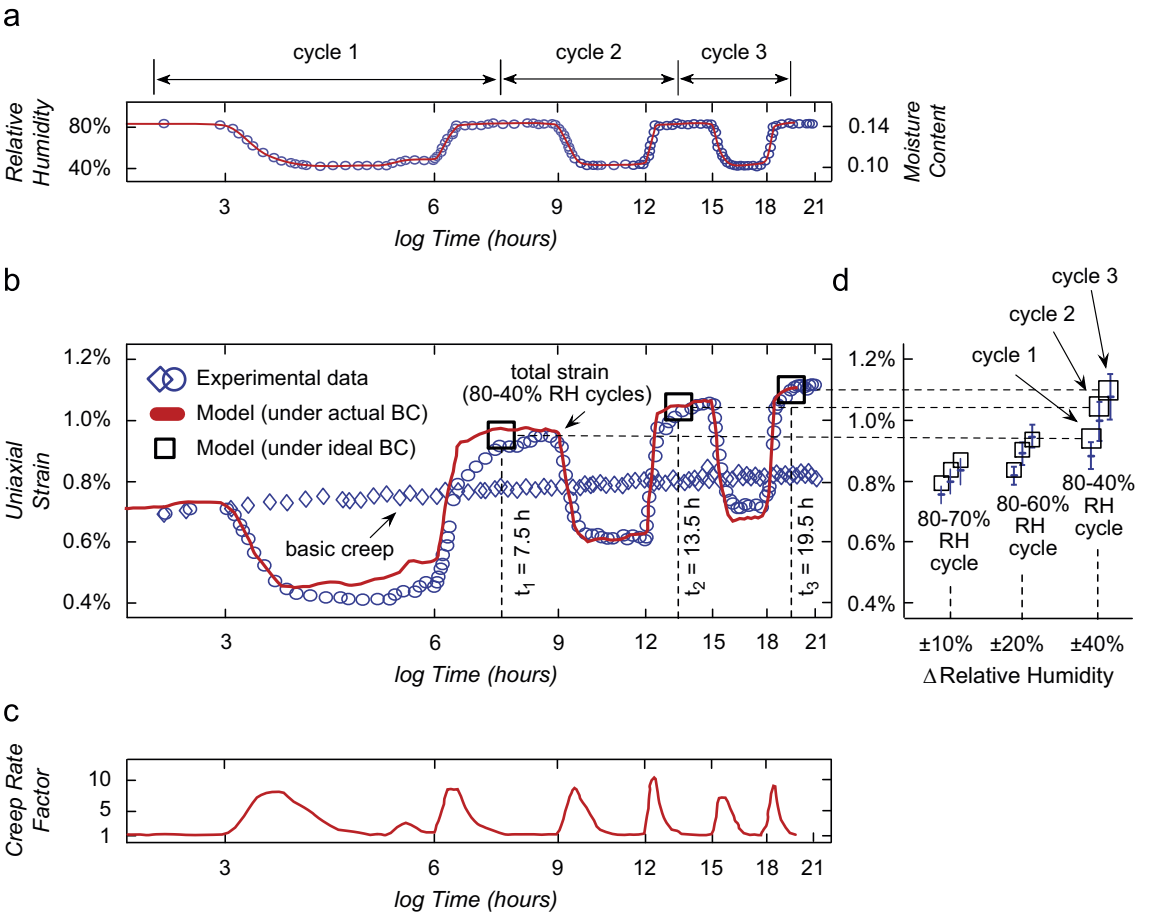

Fig. 3. Experimental creep measurements of thin paper sheets exposed to relative humidity (RH) cycles, along with fits and predictions obtained with our model (data digitized from Alfthan, 2004). The model is summarized by Eqs. (2)–(4). Detailed numerical procedure is given in Appendix B. (a) Ambient RH during cycles between 80% and 40% (blue circles) and the resulting average macropore RH in the specimen (red line) calculated using our fluid transport model. Equivalent moisture content also shown at right. (b) Uniaxial strain under constant (blue diamonds at 80% RH) and variable (blue circles at cyclic 80–40% RH) ambient conditions, along with a fit obtained from our model (red line). To obtain the fit, only the hygral expansion coefficient ($\beta = 0.10$) and the transient creep constant from Eq. (4) ($k = 0.23\ \mathrm{m^3\ s\ kg^{-1}}$) were varied. Only the latter is responsible for the final difference between the strains under constant and variable RH (hygral strain is elastic). (c) Average creep rate factor in the cross-section from the model fit in (b). Consistency with values of other materials in Fig. 1 reinforces the argument for a common transient creep mechanism among different materials. (d) Predictions of total strain of paper sheets exposed to 80–70% RH and 80–60% RH cycles, at time stations t_1, t_2, and t_3. No model parameters were changed from (b) except the prescribed boundary conditions (BC), i.e. the ambient RH. Good agreement is found between the experimentally reported strains (blue error bars) and predicted values (black open squares). Idealized (rather than reported) BC were used in calculations for lack of reported data; however, little difference between the two exists as evident from the 80% to 40% RH cycles in (b). (For interpretation of the references to color in this figure legend, the reader is referred to the web version of this article.)

Fig. 3b are shown in Fig. 3c. The results for paper are consistent with values calculated from experimental data from other materials such as cement paste, wood, and Kevlar-epoxy composite (compare Fig. 1 and Fig. 3c), reinforcing the argument for a common mechanism among different materials.

5. Final discussion

Given the very physical basis of our model and its broad agreement with experimental data, we argue that the results provide a confirmation that the nanoscale movement of water enhances the internal lubrication of the studied materials, previously described as loosening of the hydrogen bonds, and that this is the primary source of viscous softening. At once, this also suggests that both the accelerated and basic creep, i.e. viscous strain under changing and constant MC, are of common origin.

We note that our validation in Fig. 3 is approximate in its detail because we used a very simple linear description of shear-thinning of nano-confined water in Eq. (4) while molecular dynamics experiments on various lubricants indicate a logarithmic dependence. Nevertheless, we confirmed that the same basic form of the result is obtained with more complex constitutive descriptions. Based on the experimental studies outlined in Section 4, and our modeling experience of thin

paper sheets, we suggest that the most fruitful size-range for future studies of the transient phenomena is below 1 cm specimen thickness (the thinner the better). Particular emphasis should be placed on testing the same material for a range of thicknesses. To our knowledge, such tests are not available in the literature. The tests would at once help minimize the effects of differential stresses due to short drying/wetting times, which helps isolate the transient creep, and attack the problem of size effect, which comes to prominence at small specimen thickness (see Sections 3.2 and 4.1). Thin sheets or individual fibers appear best suited for the task.

Finally, we note that viscosity of solids is a property that enables the materials to dissipate as opposed to simply absorb energy. This is also what makes viscous materials in general less sensitive to the presence of random defects at the expense perhaps being too deformable. Therefore, to be able to temporarily (and significantly) 'soften' under quickly changing moisture environments while remaining resistant at other times, something that the materials discussed in this work do so well, can be an extremely useful property whose basic principles should find application in small-scale structural systems.

Acknowledgments

This work was partly supported by the Initiative for Sustainable Energy at Northwestern University, the US DOE Grant no. DE-FG02-08ER15980, the US AFOSR Grant no. FA9550-08-1-1092, and the US NSF Grant no. CMMI-1060087. This support is gratefully acknowledged. I.V. would also like to thank Dr. Jia-Liang Le for his insight on the topic of size effect during the preparation of the paper. We also thank the anonymous reviewers for their insight on polymeric materials and generally constructive comments aimed at improving the paper.

Appendix A. Flow in a partially saturated, double porosity medium

As described in Section 3, a general description of flow in a saturated dual porosity system takes the following form:

$$\frac{\partial w_1}{\partial t} + \operatorname{div} \rho V_1 - q^* = 0 \tag{A.1a}$$

$$\frac{\partial w_2}{\partial t} + \operatorname{div} \rho V_2 + q^* = 0 \tag{A.1b}$$

where q^* represents the 'interflow' or the rate of fluid exchange between the two porous systems and ρ is the liquid water density.

Two pore systems here are macropores (subscript 1) and sites of secondary bonding or nanopores (subscript 2). Macropores are partially saturated, with transport described by Fick's law. The nanopores remain fully saturated for all but extremely low partial pressures (as discussed in the text), with transport described by Darcy's law. Thus w_1 and V_1 are the water vapor concentration and water vapor flow velocity in the macropores, while w_2 and V_2 are the liquid water concentration and the liquid water flow velocity in the nanopores. These definitions lead to the following expressions:

$$w_1 = \rho\phi_1 \left[h_1 p_v^{sat} \frac{M}{RT} \right] \quad \text{water vapor (kg m}^{-3}\text{)} \tag{A.2a}$$

$$w_2 = \rho\phi_2 \quad \text{liquid water (kg m}^{-3}\text{)} \tag{A.2b}$$

$$V_1 = -\frac{\mathfrak{D}_1}{\rho} \operatorname{grad} w_1 \quad \text{Fick (m s}^{-1}\text{)} \tag{A.2c}$$

$$V_2 = -\frac{\kappa_2}{\mu_2} \operatorname{grad} p_2 \quad \text{Darcy (m s}^{-1}\text{)} \tag{A.2d}$$

$$q^* = \frac{\alpha}{\mu_2}(p_2 - p_1), \quad \alpha = \frac{\kappa_2}{l^2} \quad \text{Barenblatt–Zheltov (kg m}^{-3}\text{ s}^{-1}\text{)} \tag{A.2e}$$

$$p_1 = \frac{RT}{M} \ln h_1 \quad \text{Kelvin–Laplace (N m}^{-2}\text{)} \tag{A.2f}$$

$$p_v^{sat} = p_v^{ref} \exp\left[\frac{\Delta H_{vap}}{R} \left(\frac{1}{T^{ref}} - \frac{1}{T} \right) \right] \quad \text{Clausius–Clapeyron (N m}^{-2}\text{)} \tag{A.2g}$$

$$h_1 = \text{macropore relative humidity} \tag{A.2h}$$

$$p_2 = \text{nanopore liquid pressure} \tag{A.2i}$$

The constants are the ideal gas constant R, the molar volume of water M, the heat of water vaporization ΔH_{vap}, and the reference saturated water vapor pressure p_v at a corresponding temperature T^{ref}. The material parameters are the

temperature T [K], porosity of the macropores (ϕ_1) and of the nanopores (ϕ_2), the vapor diffusion constant for the macropores $\mathfrak{D}_1$ [$m^2\,s^{-1}$], the permeability constant for the nanopores κ_2 [m^2], the dynamic water viscosity at the nanoscale μ_2 [$N\,s\,m^{-2}$], the dimensionless geometric characteristic of the nanoporous medium α that describes how easily the fluid can exchange between the two porous regions, and l [m], an intrinsic length scale or dimension of the porous matrix (Barenblatt et al., 1960).

Substituting Eqs. (A.2) into Eqs. (A.1) leads to the following coupled partial differential equations in 1D:

$$0 = S_1^0 \frac{\partial h_1}{\partial t} - d_1 D_1^0 S_1^0 \frac{\partial^2 h_1}{\partial x^2} - \frac{D_2^0}{l^2 d_2}\left(p_2 - \frac{RT}{M}\ln h_1\right) \tag{A.3a}$$

$$0 = S_2^0 \frac{\partial p_2}{\partial t} - \frac{D_2^0}{d_2}\frac{\partial^2 p_2}{\partial x^2} + \frac{D_2^0}{l^2 d_2}\left(p_2 - \frac{RT}{M}\ln h_1\right) \tag{A.3b}$$

$$S_1^0 = \phi_1 p_v^{sat} M/(RT) \tag{A.3c}$$

$$S_2^0 = \phi_2 c_f \tag{A.3d}$$

$$D_1^0 = \mathfrak{D}_1^{sat} \tag{A.3e}$$

$$d_1 = \mathfrak{D}_1/\mathfrak{D}_1^{sat} \tag{A.3f}$$

$$D_2^0 = \kappa_2^{sat}/\mu^{bulk} \tag{A.3g}$$

$$d_2 = \mu_2/\mu^{bulk} \tag{A.3h}$$

where the superscripts *sat* and *bulk* refer to the saturated and the bulk properties respectively; c_f is the nanoscale fluid compressibility. It is helpful to make Eqs. (A.3) non-dimensional for the added benefit of linearizing the logarithmic terms. To this end, we adopt a 1D boundary value problem shown in Fig. 2c. The initial and the boundary relative humidity are given by values h^i and h^b (p_1^i and p_1^b are the corresponding liquid pressures); L is the half-length of the cross-section. Adopting the following dimensionless variables:

$$\theta = \frac{D_1^0}{L^2} t \tag{A.4a}$$

$$y = \frac{x}{L} \tag{A.4b}$$

$$f = \frac{\ln h_1 - \ln h^i}{\ln h^b - \ln h^i} \tag{A.4c}$$

$$g = \frac{p_2 - p_1^i}{p_1^b - p_1^i} = \frac{p_2 - (RT/M)\ln h^i}{(RT/M)\ln h^b - (RT/M)\ln h^i} \tag{A.4d}$$

and substituting Eqs. (A.4) into Eqs. (A.3) leads to the following coupled non-dimensional differential equations of parabolic type:

$$\left(\frac{\partial f}{\partial \theta}\right) - d_1\left(\frac{\partial^2 f}{\partial y^2}\right) - \frac{1}{d_2}\frac{L^2}{l^2}\frac{D_2^0}{h_1 S_1^0 D_1^0}\frac{RT}{M}(g-f) = 0 \tag{A.5a}$$

$$\frac{S_2^0}{h_1 S_1^0}\frac{RT}{M}\left(\frac{\partial g}{\partial \theta}\right) - \frac{1}{h_1 S_1^0}\frac{D_2^0}{d_2 D_1^0}\frac{RT}{M}\left(\frac{\partial^2 g}{\partial y^2}\right) + \frac{1}{d_2}\frac{L^2}{l^2}\frac{D_2^0}{h_1 S_1^0 D_1^0}\frac{RT}{M}(g-f) = 0 \tag{A.5b}$$

On physical grounds, we assume that the rate of permeation of the fluid via the nanopores is negligible, such that equilibration of internal humidity levels primarily takes place via the interflow fluid exchange between the macropores and the nanopores. Taking this simplification into account, Eqs. (A.5) reduce to

$$\left(\frac{\partial f}{\partial \theta}\right) - d_1\left(\frac{\partial^2 f}{\partial y^2}\right) + \frac{S_2^0}{h_1 S_1^0}\frac{RT}{M}\left(\frac{\partial g}{\partial \theta}\right) = 0 \tag{A.6a}$$

$$\left(\frac{\partial g}{\partial \theta}\right) + \frac{1}{d_2}\frac{L^2}{l^2}\frac{D_2^0}{S_2^0 D_1^0}(g-f) = 0 \tag{A.6b}$$

where values indicated by h_1, d_1, and d_2 represent the non-linear contributions (see Eqs. (A.2) and (A.3) for definition). Incorporating both space y (k nodes) and time θ (n time steps) into a finite difference routine, the space

gradients[2] and time derivatives become

$$\frac{\partial f}{\partial \theta}=\frac{f^{n+1}-f^{n}}{\theta^{n+1}-\theta^{n}},\quad \frac{\partial g}{\partial \theta}=\frac{g^{n+1}-g^{n}}{\theta^{n+1}-\theta^{n}} \tag{A.7a}$$

$$\frac{\partial^2 f}{\partial y^2}=4\left[\frac{f_{k+1}-2f_k+f_{k-1}}{(y_{k+1}-y_{k-1})^2}\right],\quad \frac{\partial^2 g}{\partial y^2}=4\left[\frac{g_{k+1}-2g_k+g_{k-1}}{(y_{k+1}-y_{k-1})^2}\right] \tag{A.7b}$$

while the entire problem can be cast as a vector residual in terms of the following global matrices (square brackets) and vectors (curly brackets):

$$\{R\}=[\mathbb{R}_1]\{F^{n+1}\}-[\mathbb{R}_0]\{F^{n}\} \tag{A.8a}$$

where

$$\{F\}=\{f_1,f_2,\ldots f_k,g_1,g_2,\ldots g_k\}^T \tag{A.8b}$$

$$[\mathbb{R}_1]=[\mathbb{R}_1(\{F^{n+1}\})] \tag{A.8c}$$

$$[\mathbb{R}_0]=[\mathbb{R}_0(\{F^{n+1}\})] \tag{A.8d}$$

Eqs. (A.8) are solved iteratively (r iterations) via a fully implicit Newton–Raphson routine (backward Euler), until the norm of the residual $\{R\}$ is minimized to a specified tolerance:

$$\{F\}^{r=0}=\{F\}^{n} \tag{A.9a}$$

$$\{F\}^{r+1}=\{F\}^{r}-\left[\frac{\partial\{R\}}{\partial\{F\}^{r}}\right]^{-1}\{R(\{F\}^{r})\} \tag{A.9b}$$

If non-linear, the gradient of the residual $\{R\}$ and the matrices $[\mathbb{R}_1]$ and $[\mathbb{R}_0]$ are 'frozen' at each iteration, leading to $\partial\{R\}/\partial\{F\}^{r}=[\mathbb{R}_1(\{F^{r}\})]$. In this work, time stepping was performed in logarithmic θ increments while y nodes were spaced linearly and uniformly.

Appendix B. Thin paper sheets: model parameters

In total, two parameters were varied in order to produce the values shown in Fig. 3:

Constitutive multiplier k: The constitutive law is fundamentally a macroscopic one, and thus requires an empirical constant.

Hygral expansion coefficient β: Release (uptake) of moisture in a freely dried (wetted) paper generally results in no irreversible strain. β relates the change in relative humidity with the change in elastic strain. The calibrated value of $\beta=0.10$ used in the work is on par with published values of other paper types (Uesaka, 1994; Alava and Niskanen, 2006).

An additional parameter, the storage capacity of the nanosites S_2^0, was implicitly inferred from experimental observations (Kubát and Lindbergson, 1965). The researchers noted that the mechanical damping of thin paper sheets did not immediately return to its equilibrium value upon completion of (macro)pore drying. Instead, the steady-state equilibrium in damping was reached "within hours", an indication of the delay in internal equilibrium. In the transport equations in Eq. (A.6b), holding all other material parameters constant, S_2^0 controls the extent of this time lag. To match the experiments in Kubát and Lindbergson (1965) to similar order of magnitude, we estimate the value of S_2^0 to be on the order of $1e-21\ m^2\ N^{-1}$. Fig. 2d shows the resulting breakthrough curve. $S_2^0=\phi_2 c_f$ is a physically meaningful quantity. Its value suggests that either the volume porosity of the nanosites ϕ_2 is extremely low in comparison to the porosity of the macropores and/or that the compressibility of pore water at the nanoscale c_f is orders of magnitude less than the bulk water.

All other material parameters are adopted from direct physical considerations, as outlined in Eqs. (B.1). Paper used in testing was isotropic hand sheet, made of unbleached and beaten softwood sulphate pulp (Alfthan, 2004). MC varies nearly linearly with relative humidity (RH) in the range of 40–80% RH. The applied specific stress (stress per density) during the creep test was 4.9 kN m kg^{-1}, which corresponds to about 1/8 of the maximum tensile strength at 50% RH. All calculated values shown in Fig. 3 are averages over the entire cross-section, containing 40 evenly spaced nodes in a finite difference routine and 20 log-spaced time steps for every 0.25% jump in ambient relative humidity.

macropores:

$$S_1^0=1.301e-05 \tag{B.1a}$$

$\phi_1=0.622$ (estimate per basis weight (17 g m^{-2}) (Alfthan, 2004), relative fiber density (1.50) (Alfthan, 2004), and paper thickness (30e−6 m) Alava and Niskanen, 2006)

[2] Note that in the simplified Eqs. (A.6), the second order gradient of the nanopore fluid pressure is null, or rather $\partial^2 g/\partial y^2\approx 0$.

$p_v^{sat} = 2.827\text{e}3\ \text{N m}^{-2}$

$M = 1.802\text{e}{-5}\ \text{m}^3\ \text{mol}^{-1}, \quad R = 8.314\ \text{J K}^{-1}\ \text{mol}^{-1}, \quad T = 293\ \text{K}$

$D_1^0 \approx 2\text{e}{-12}\ \text{m}^2\ \text{s}^{-1}$ (untreated sulphate paper Ebrahimzadeh and Bertilsson, 1998, Table 1) (B.1b)

$d_1 = 1$ (macrodiffusion multiplier) (B.1c)

nanosites and interflow:

$S_2^0 \approx 1\text{e}{-21}\ \text{m}^2\ \text{N}^{-1}$ (see preceding text for explanation) (B.1d)

$D_2^0 = 1\text{e}{-21}\ \text{m}^4\ \text{N}^{-1}\ \text{s}^{-1}, \quad \alpha = k_2/l^2 = 1\text{e}{-6}$ (B.1e)

$\kappa_2 = 1\text{e}{-24}\ \text{m}^2$ (nanoscale permeability of cement Powers, 1958, with same order of magnitude presumed for paper as well) (B.1f)

$l = 1\text{e}{-9}\ \text{m}$ (intrinsic lengthscale of a porous matrix) (B.1g)

$\mu_{bulk} = 1\text{e}{-3}\ \text{N s m}^{-2}$ (B.1h)

$d_2 = 1\text{e}{+3}$ (nanoviscosity multiplier Li et al., 2007; Riedo, 2007) (B.1i)

geometry and initial/boundary conditions:

$L = 1.5\text{e}{-5}\ \text{m}$ (based on 17 g m^{-2} basis weight, Alava and Niskanen, 2006, Fig. 18) (B.1j)

$h_i = 0.80$ RH ($\approx$ 0.140 MC) (per experimental procedure, Alfthan, 2004) (B.1k)

$h_b = 0.40, 0.60, 0.70$ RH ($\approx 0.100, 0.125, 0.130$ MC) (B.1l)

model parameters:

$k = 0.23\ \text{s}\ (\text{kg m}^{-3})^{-1}$ (B.1m)

$\beta = 0.10$ (B.1n)

References

Alava, M., Niskanen, K., 2006. The physics of paper. Rep. Prog. Phys. 69 (3), 669.
Alfthan, J., 2004. The effect of humidity cycle amplitude on accelerated tensile creep of paper. Mech. Time-Dependent Mater. 8 (4), 289–302.
Algie, J.E., Watt, I.C., 1965. The effect of changes in the relative humidity on the electrical conductivity of wool fibers. Text. Res. J. 35 (10), 922–929.
Algie, J., Downes, J., Mackay, B., 1960. Electrical conduction in keratin. Text. Res. J. 30 (6), 432–434.
Armstrong, L.D., 1972. Deformation of wood in compression during moisture movement. Wood Sci. 5 (2), 81–86.
Armstrong, L.D., Christensen, G.N., 1961. Influence of moisture changes on deformation of wood under stress. Nature 191 (4791), 869–870.
Armstrong, L.D., Kingston, R.S.T., 1960. Effect of moisture changes on creep in wood. Nature 185 (4716), 862–863.
Armstrong, L.D., Kingston, R.S.T., 1962. The effect of moisture content changes on the deformation of wood under stress. Aust. J. Appl. Sci. 13 (4), 242–256.
Atkinson, T.S., Ewers, B.J., Haut, R.C., 1999. The tensile and stress relaxation responses of human patellar tendon varies with specimen cross-sectional area. J. Biomech. 32 (9), 907–914.
Bažant, Z.P., Chern, J.C., 1985. Concrete creep at variable humidity: constitutive law and mechanism. Mater. Struct. 18 (1), 1–20.
Bažant, Z.P., Xi, Y., 1994. Drying creep of concrete: constitutive model and new experiments separating its mechanisms. Mater. Struct. 27 (1), 3–14.
Bažant, Z.P., Asghari, A.A., Schmidt, J., 1976. Experimental study of creep of hardened portland cement paste at variable water content. Mater. Struct. 9 (4), 279–290. (figure 19).
Barenblatt, G.I., Zheltov, Y.P., 1960. On fundamental equations of flow of homogeneous liquids in naturally fractured rocks. Dokl. Akad. Nauk USSR 132 (3), 545–548. (in Russian).
Barenblatt, G.I., Zheltov, I.P., Kochina, I.N., 1960. Basic concepts in the theory of seepage of homogeneous liquids in fissured rocks [strata]. J. Appl. Math. Mech. 24 (5), 1286–1303.
Byrd, V.L., 1972. Effect of relative humidity changes during creep on handsheet paper properties. Tappi J. 55 (2), 247–252.
Chen, Z.X., 1989. Transient flow of slightly compressible fluids through double-porosity, double-permeability systems—a state-of-the-art review. Transp. Porous Media 4 (2), 147–184.
Chimich, D., Shrive, N., Frank, C., Marchuk, L., Bray, R., 1992. Water content alters viscoelastic behaviour of the normal adolescent rabbit medial collateral ligament. J. Biomech. 25 (8), 831–837.
Danilatos, G.D., Postle, R., 1981. Low-strain dynamic mechanical properties of keratin fibers during water absorption. J. Macromol. Sci. Part B: Physics 19 (1), 153–165.
Dounis, D.V., Moreland, J.C., Wilkes, G.L., Dillard, D.A., Turner, R.B., 1993. The mechano-sorptive behavior of flexible water-blown polyurethane foams. J. Appl. Polym. Sci. 50 (2), 293–301.
Ebrahimzadeh, P.R., Bertilsson, H., 1998. Effect of impregnation on mechanosorption in wood and paper studied by dynamic mechanical analysis. Wood Sci. Technol. 32 (2), 101–118.
Feughelman, M., 1962. A note on mechanical weakening in a stretched wool fiber during moisture sorption. Text. Res. J. 32 (9), 788–789.
Garner, E., Lakes, R., Lee, T., Swan, C., Brand, R., 2000. Viscoelastic dissipation in compact bone: implications for stress-induced fluid flow in bone. J. Biomech. Eng. 122 (2), 166–172.
Gibson, E.J., 1965. Creep of wood: role of water and effect of a changing moisture content. Nature 206 (4980), 213–215.

Habeger, C.C., Coffin, D.W., Hojjatie, B., 2001. Influence of humidity cycling parameters on the moisture-accelerated creep of polymeric fibers. J. Polym. Sci. Part B: Polym. Phys. 39 (17), 2048–2062.
Haut, T.L., Haut, R.C., 1997. The state of tissue hydration determines the strain-rate-sensitive stiffness of human patellar tendon. J. Biomech. 30 (1), 79–81.
Haygreen, J., Hall, H., Yang, K.-N., Sawicki, R., 1975. Studies of flexural creep behavior in particleboard under changing humidity conditions. Wood Fiber Sci. 7 (2), 74–90.
Jop, P., Forterre, Y., Pouliquen, O., 2006. A constitutive law for dense granular flows. Nature 441 (7094), 727–730.
Kubát, J., Lindbergson, B., 1965. Damping transients in polymers during sorption and desorption. J. Appl. Polym. Sci. 9 (8), 2651–2654.
Lane, J.M.D., Chandross, M., Stevens, M.J., Grest, G.S., 2008. Water in nanoconfinement between hydrophilic self-assembled monolayers. Langmuir 24 (10), 5209–5212.
Leng, Y., Cummings, P.T., 2005. Fluidity of hydration layers nanoconfined between mica surfaces. Phys. Rev. Lett. 94 (2), 026101.
Li, T.-D., Gao, J., Szoszkiewicz, R., Landman, U., Riedo, E., 2007. Structured and viscous water in subnanometer gaps. Phys. Rev. B 75 (11), 115415.
Liou, W.J., 1998. Effects of moisture content on the creep behavior of nylon-6 thermoplastic composites. J. Reinf. Plast. Compos. 17 (1), 39–50.
Mackay, B.H., Downes, J.G., 1959. The effect of the sorption process on the dynamic rigidity modulus of the wool fiber. J. Appl. Polym. Sci. 2 (4), 32–38.
Major, R.C., Houston, J.E., McGrath, M.J., Siepmann, J.I., Zhu, X.Y., 2006. Viscous water meniscus under nanoconfinement. Phys. Rev. Lett. 96 (17), 177803.
Manias, E., Bitsanis, I., Hadziioannou, G., Brinke, G.t., 1996. On the nature of shear thinning in nanoscopically confined films. Europhys. Lett. 33 (5), 371–376.
Mooney, D., MacElroy, J., 2007. Differential water sorption studies on Kevlar 49 and as-polymerized poly(p-phenylene terephthalamide): determination of water transport properties. Langmuir 23 (23), 11804–11811.
Nordon, P., 1962. Some torsional properties of wool fibers. Text. Res. J. 32 (7), 560–568.
Olsson, A.-M., Salmén, L., Eder, M., Burgert, I., 2007. Mechano-sorptive creep in wood fibres. Wood Sci. Technol. 41 (1), 59–67.
Pérez-Rigueiro, J., Viney, C., Llorca, J., Elices, M., 2000. Mechanical properties of silkworm silk in liquid media. Polymer 41 (23), 8433–8439.
Pickett, G., 1942. The effect of change in moisture-content of the creep of concrete under sustained load. J. Am. Concr. Inst. 13 (4), 333–355.
Powers, T.C., 1958. Structure and physical properties of hardened portland cement paste. J. Am. Ceram. Soc. 41 (1), 1–6.
Riedo, E., 2007. Water behaves like a viscous fluid on the nano-scale. Membr. Technol. 2007 (8), 8.
Ritchie, J., Smith, C., Bell, F.I., McEwen, I.J., Viney, C., 2005. Effects of wetting and desiccation on the creep properties of spider dragline silk. In: Ulm, Viney, C., Katti, K., Hellmich, C. (Eds.), Mechanical Properties of Bioinspired and Biological Materials, Materials Research Society, Warrendale, PA, pp. 125–130.
Söremark, C., Fellers, C., 1993. Mechano-sorptive creep and hygroexpansion of corrugated board in bending. J. Pulp Pap. Sci. 19 (1), J19–J26.
Sasaki, N., Enyo, A., 1995. Viscoelastic properties of bone as a function of water content. J. Biomech. 28 (7), 809–815.
Sendner, C., Horinek, D., Bocquet, L., Netz, R.R., 2009. Interfacial water at hydrophobic and hydrophilic surfaces: slip, viscosity, and diffusion. Langmuir 25 (18), 10678–10781.
Smith, C., Ritchie, J., Bell, F.I., McEwen, I.J., Viney, C., 2003. Creep and low strength of spider dragline subjected to constant loads. J. Arachnology 31 (3), 421–424.
Tanioka, A., Jojima, E., Miyasaka, K., Ishikawa, K., 1973. Effect of water on the mechanical properties of collagen films. J. Polym. Sci. Polym. Phys. Ed. 11 (8), 1489–1502.
Thornton, G.M., Shrive, N.G., Frank, C.B., 2001. Altering ligament water content affects ligament pre-stress and creep behaviour. J. Orthop. Res. 19 (5), 845–851.
Uesaka, T., 1994. General formula for hygroexpansion of paper. J. Mater. Sci. 29 (9), 2373–2377.
Urbakh, M., Klafter, J., Gourdon, D., Israelachvili, J., 2004. The nonlinear nature of friction. Nature 430 (6999), 525–528.
Urbanik, T., 1995. Hygroexpansion-creep model for corrugated fiberboard. Wood Fiber Sci. 27 (2), 134–140.
Vandamme, M., Ulm, F.-J., 2009. Nanogranular origin of concrete creep. Proc. Natl. Acad. Sci. USA 106 (26), 10552–10557.
Wang, J.Z., Dillard, D.A., Wolcott, M.P., Kamke, F.A., Wilkes, G.L., 1990. Transient moisture effects in fibers and composite materials. J. Compos. Mater. 24 (9), 994–1009.
Wang, J.Z., Dillard, D.A., Kamke, F.A., 1991. Transient moisture effects in materials. J. Mater. Sci. 26 (19), 5113–5126. http://dx.doi.org/:10.1007/BF01143201.
Wang, J.Z., Dillard, D.A., Ward, T.C., 1992. Temperature and stress effects in the creep of aramid fibers under transient moisture conditions and discussions on the mechanisms. J. Polym. Sci. Part B: Polym. Phys. 30 (12), 1391–1400.